Torsional Stiffness Optimization in Heavy Commercial Vehicle Chassis Platforms: A Review of FEA-Based Design, Optimization Methods and Research Gaps

Abhishek Deshmukh[1] P. G. Sarasambi[2] S. D. Shinde[3]
[1]Research Scholar [2]Assistant Professor [3]HOD & Principal
[1,2,3]Department of Mechanical Engineering (Design Engineering)
[1,2]Shree Ramchandra College of Engineering, Pune, India

Abstract — Heavy commercial vehicle (HCV) ladder chassis frames must carry payload, cab and powertrain loads while resisting severe twisting when wheels on opposite sides move vertically in opposite directions on unpaved or mining terrain. Insufficient torsional stiffness degrades handling, shifts steering geometry, overloads cross-member joints and accelerates fatigue cracking. This paper reviews finite element analysis (FEA), surrogate-assisted multi-objective optimization and experimental validation practice for thin-walled load-carrying structures (ladder chassis, crane, telehandler and forklift booms) and assesses its transferability to HCV chassis. Reported mass reductions from optimization of comparable structures range from 8.44% to 12.5%. A small-scale case study of a C40 mild-steel transmission shaft (Ø10 mm × 70 mm, 1470 N·mm) is used to demonstrate an analytical–numerical–experimental validation chain and its limitations. Eight research gaps are identified, including the scarcity of direct HCV chassis torsional optimization studies, simplified joint-contact modelling, omission of buckling and fatigue from the optimization loop, limited strain-gauge validation, and inconsistent dynamic load factors (1.15–1.5). A nine-step FEA-based optimization workflow addressing these gaps is proposed.

Keywords: Heavy Commercial Vehicle; Ladder Chassis; Torsional Stiffness; Finite Element Analysis; Surrogate Modelling; NSGA-II; Lightweight Design; Fatigue

I. Introduction

Heavy commercial vehicles (HCVs), including multi-axle tipper trucks, long-haul freight carriers and construction vehicles, underpin mining, infrastructure logistics and bulk freight. The ladder chassis is the structural backbone of such vehicles: it supports the powertrain, cab and cargo body and absorbs the dynamic loads transmitted from the road. Among the loading modes it experiences, torsion is one of the most severe. When one-wheel rides over a bump while the opposite wheel drops, the frame is twisted about its longitudinal axis, and this twist is resisted mainly by the side rails, the cross-members and the joints between them.

Inadequate torsional stiffness has several consequences:

- degraded directional handling and altered front-wheel steering geometry;
- transient wheel-load imbalance;
- low-cycle fatigue initiation at cross-member gussets and bracket cut-outs; and
- distortion of the mounting plates of chassis-mounted sub-systems (driveline, actuation and sensing units), leading to misalignment.

Increasing stiffness by adding material, however, raises frame mass, reducing payload capacity and affecting stability. The design problem is therefore to maximize torsional stiffness per unit mass while satisfying stress, buckling, fatigue and vibration limits.

The objectives of this paper are to: (i) summarize the structure, load cases and failure modes of HCV chassis; (ii) survey FEA modelling and optimization practice in comparable structures; (iii) present an analytical–numerical–experimental cross-check on a chassis-mounted shaft and worm-gear sub-system; (iv) identify research gaps; and (v) propose a nine-step optimization workflow.

II. Chassis Structure, Loading and Failure Modes

A. Structure and load path

A typical HCV chassis comprises two longitudinal side members of C-channel or top-hat section, joined by transverse cross-members and gusset joints. Loads from payload, cab and powertrain enter the side rails through suspension brackets. The functional roles of the principal elements are summarized in Table 1. Because open sections are efficient in vertical bending but inherently compliant in torsion, joint design strongly governs global torsional stiffness.

Element	Function
Longitudinal side members	Carry the main bending moment from payload and dead weight
Cross-members	Connect the side rails; resist lateral forces and carry torsional shear flow
Gussets and bolted/welded joints	Prevent local section warping at junctions
Support bearings and linkages	Maintain alignment of mounted shafts and actuation hardware under twist

Table 1: Principal structural elements of an HCV ladder chassis

B. Load cases

The load cases commonly used in chassis and box-section optimization studies are listed in Table 2. The reported dynamic impact factors span 1.15 to 1.5, which complicates comparison between studies.

Load case	Description
Maximum torsional twist	Bump on one side and droop on the other, producing maximum longitudinal twist
Dynamic impact	Rated payload multiplied by a dynamic factor (reported range 1.15–1.5)
Lateral / side load	Cornering or side-slope forces causing combined bending and torsion
Vertical plus braking	Full payload with longitudinal deceleration and braking reaction torques

Table 2: Typical load cases for HCV chassis

All rights reserved by www.ijsrd.com

C. Failure modes, materials and standards

The principal failure modes are yielding at stress concentrations (suspension brackets, cross-member cut-outs), local buckling of thin-walled channels, torsional warping, and fatigue cracking at welded joints under cyclic loading. HCV frames use high-strength structural steels, broadly in the Q235–Q460 range or equivalent Domex/Strenx grades. Higher strength permits thinner walls and lower mass, but increases susceptibility to local buckling and weld-fatigue sensitivity. Torsional stiffness requirements are driven indirectly by safety and stability regulation, including UNECE requirements and stability-verification standards such as the ISO 22915 series, because excessive twist alters the alignment of mechanical components at full legal payload.

III. Review of Related Work

A. Actuation, sensing and driveline-related studies

A first group of studies addresses electromechanical actuation and sensing hardware mounted on vehicle structures. Thivagar investigated compact motor-driven actuation with electronic proximity sensing, reporting reduced operator effort and fewer human errors. Raghunath Reddy and Naidu applied computer-aided stress analysis to hydraulic cylinder components and stressed the importance of material selection under multi-axial loading. Dharia and Bhopale, and Nayak, examined electromechanical actuators that replace manual levers and cables, improving packaging flexibility and locking reliability. More reported that high-rigidity solid shafts retain fail-safe behaviour after long standby periods. Kotalwar and Harje, and Joy et al., studied assist systems, with the latter reporting response-delay reductions of up to 20% from stiffer mechanical connections in track tests. Thakur et al. implemented FPGA-based control using ultrasonic echo sensing; Saini and Joshi studied inclination-sensor-based holding devices; Belhocine et al. used 3D finite element models to relate non-uniform contact pressure to wear and squeal; and Wakchaure et al. showed that inertial overshoot in motor-driven systems produces peak loads that require current cut-off logic.

These studies are relevant chiefly because chassis-mounted sub-systems depend on the frame not distorting their mounts: frame torsional stiffness is an enabling requirement for their reliable operation.

B. FEA and optimization of thin-walled load-carrying structures

Direct studies of HCV ladder-chassis torsional optimization are scarce, so the literature on booms and comparable thin-walled structures is the principal source of methods. Table 3 summarizes the studies compiled for this review.

Structure	Analysis	Outcome
Telehandler / heavy vehicle	Static FEA; plate and beam elements	Strengthened for 1.5 dynamic factor
Telehandler chassis	Static FEA; five load cases	Redesign at failing hinge points
Telescopic platform	Modal FEA and experimental modal test	Vibration standards met
Aerial-lift boom	Kriging metamodel; topology optimization	Two-phase lightweight frame design
Crane boom (35 t)	ANSYS static vs. hand calculation	Peak stress and deflection hot-spots identified
Telescopic jib arm	ANSYS FEM with experiment	Optimum cross-section shape
Truck-crane contact zone	Analytical model, FEM and rig test	Box-segment design guidelines
Thin-walled structure	ABAQUS static and buckling	Thickness optimization in six iterations
Tower-crane boom (Jia & Wan)	APDL static FEA; fuzzy-genetic algorithm	≈ −11.6% mass (−309 kg)
Rescue arm	ANSYS static and fatigue	Lightweight parameter optimization
Telescopic boom	ANSYS static and linear buckling	Pad-contact theory vs. FE verification
Crane welded joints	Sub-model FEA; S–N fatigue	Fatigue life assessment (no optimization)
300 t crane boom	ANSYS, static test, modal	Response-surface lightweighting
Truck-crane boom	Static FEA; slide-pad stress	Cross-section sizing via MATLAB
Compact telehandler	Bond-graph multibody dynamics	Stability-limit map
Telescopic crane (Cao et al.)	ANSYS static, fatigue, strain gauges	BO-LightGBM surrogate; digital twin
Forklift boom, 9.89 m (Sun et al.)	ANSYS static, modal, harmonic	RSM-RBFNN + NSGA-II + 3σ; −12.5% mass
Forklift cross-section (Fang et al.)	Topology and parametric FEA	Kriging + MOGA; −8.44% mass, higher stiffness

Table 3: Representative FEA and optimization studies in comparable structures

C. Quantitative outcomes and areas of agreement

Table 4 and Fig. 1 summarize the key quantitative results. Across structure types, formulations consistently use cross-section dimensions and plate thicknesses as design variables, mass as the objective, and stress, deflection and, increasingly, natural frequency as constraints. Solution strategies have progressed from direct FE-in-the-loop iteration (APDL/ABAQUS scripting) to surrogate-assisted multi-

All rights reserved by www.ijsrd.com

objective search with reliability constraints. Reported mass savings fall between about 8% and 12.5%.

Study	Application	Reported result
Jia & Wan	Tower-crane boom	−309 kg (≈ 11.6%) via fuzzy-genetic algorithm
Fang et al.	Forklift boom cross-section	−8.44% mass with enhanced torsional stiffness
Sun et al.	Forklift telescopic boom	−12.5% mass, +9.4% frequency, 3σ reliability achieved
Cao et al.	Telescopic crane	FE vs. strain-gauge error < 6.18 MPa; surrogate 0.55 s vs. 2580 s per evaluation

Table 4: Key reported quantitative results

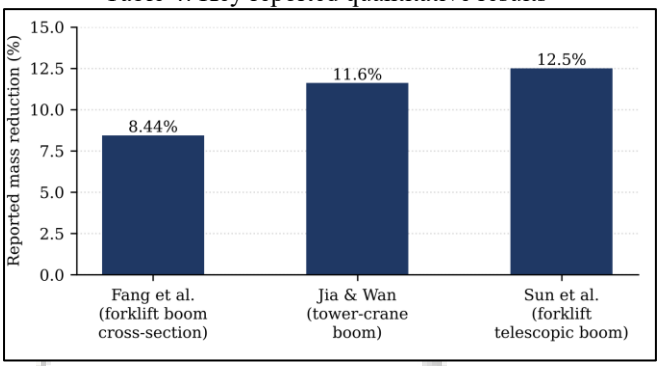


Fig. 1. Mass reductions reported for optimized boom structures in the reviewed literature.

D. FEA Modelling Practice

Element selection. Shell elements (e.g., SHELL281) are efficient for thin-walled side rails and box sections; solid elements suit brackets, pins and joint regions; beam elements idealize auxiliary shafts and cylinders.

Contact and joint treatment. The treatment of sliding pads and joints varies across studies and strongly influences local stresses (Table 5).

Approach	Remark
Explicit gap / contact elements	Captures load transfer and local overlap stresses
Analytical contact formulas	Useful when verified by rig testing
Rigid tie / multi-point constraint	Computationally efficient but hides local edge stress
Bracket and gusset reinforcement	Treats joint hot-spots as primary design drivers

Table 5: Treatment of contacts and joints in the reviewed studies

– Analysis types. Static analysis provides the baseline stress and displacement fields and must be verified against hand calculations to confirm boundary conditions. Linear buckling analysis yields critical load factors for compressed or sheared thin walls. Modal analysis ensures that natural frequencies avoid engine and road excitation. Fatigue assessment uses S–N or structural-stress methods for welds and cut-outs.

– Validation. Triaxial strain gauges, modal hammer testing and physical torsion rigs are used to validate numerical models; benchmark studies report stress correlation errors of roughly 6–9 MPa.

IV. Case Study: Validation of a Chassis-Mounted Shaft and Worm-Gear Sub-System

To illustrate the validation chain, a small torque-transmitting sub-system mounted on the chassis was examined. It consists of a C40 mild-steel shaft (Ø10 mm, length 70 mm) driven through a 1:28 worm gearbox (module 2 mm, pitch diameter 65 mm, face width 10 mm) by a 120 W, 12 V DC, 1440 rpm motor, with a peak output torque of 1470 N·mm. The isotropic material data are E = 200 GPa, ν = 0.30, G = 76.9 GPa and ρ = 7850 kg/m³.

A. Analytical evaluation

For a solid circular shaft in pure torsion,

$$T/J = \tau/R = G\varphi/L \quad (1)$$

where T is the torque, $J = \pi d^4/32$ the polar moment of area, τ the shear stress at radius R, G the shear modulus, φ the angle of twist and L the length. For $d = 10$ mm, $J = 981.75$ mm^4 and

$$\tau_{max} = T\,R/J = (1470 \times 5)/981.75 = 7.49 \text{ MPa} \quad (2)$$

$$\varphi = T\,L/(G\,J) = (1470 \times 70)/(76\,923 \times 981.75) = 1.36 \times 10^{-3} \text{ rad } (0.078°) \quad (3)$$

The twist of 1.36×10^{-3} rad corresponds to a surface displacement of $\varphi R \approx 0.0068$ mm. With an ultimate shear strength of 115 N/mm^2 and a factor of safety of 2, the allowable shear stress is 57.5 N/mm^2; the minimum diameter obtained for the adopted working force is approximately 3.14 mm, so the selected 10 mm shaft provides a large margin. The bending stress at the worm-gear tooth root, from the Lewis equation $\sigma_b = W_t/(b\,m\,Y)$ with $Y = 0.31$, $b = 10$ mm, $m = 2$ mm and an adopted tooth load of 22.6 N, is 3.65 MPa.

B. Finite element model

The geometry was modelled in CATIA V5 and analysed in ANSYS Workbench 14.5 using quadratic tetrahedral solid elements (913 elements, 1761 nodes). Cylindrical supports at the rear bearing restrained radial and axial displacement while permitting rotation, a 1470 N·mm torque was applied at the input end, and the worm-gear mesh interface was constrained. A convergence study showed a change in peak stress below 1.5% on further refinement.

C. Experimental procedure

A C40 specimen (Ø10 mm × 70 mm) was clamped coaxially in a digital torsion testing machine (EIE Instruments; 0.37 kW drive; 40 rpm head speed). After calibration and zeroing of the load display and angular encoder, the specimen was twisted in 10–20° increments, and the reactive load and surface deformation were recorded at each step. As shown in Fig. 2, the recorded load and deformation increased approximately linearly with twist angle up to 150°, from 72 to 522.8 (machine units) and from 1.919 mm to 14.342 mm respectively.

All rights reserved by www.ijsrd.com

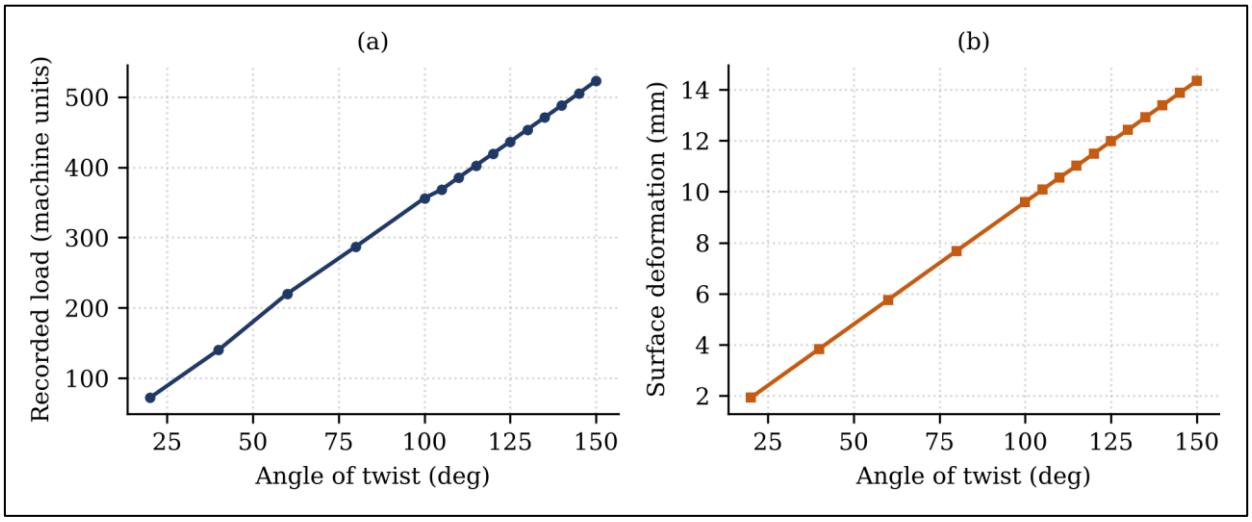


Fig. 2: Torsion test response of the C40 shaft specimen: (a) recorded load and (b) surface deformation versus angle of twist.

D. Comparison of results

Table 6 compares the three methods. Percentage differences relative to the analytical value were recomputed from the tabulated data.

Component	Method	Deformation (mm)	Stress (MPa)	Diff. vs. analytical (def. / stress)
Transmission shaft	Analytical	0.00499	7.486	—
	FEA	0.00400	10.594	−19.8% / +41.5%
	Experiment	0.00450	7.053	−9.8% / −5.8%
Worm gear	Analytical	0.00067	3.647	—
	FEA	0.00068	3.400	+1.5% / −6.8%
Full assembly	FEA	0.00353	9.059	n/a

Table 6: Comparison of analytical, FEA and experimental results

The worm-gear results agree closely. For the shaft, the FEA stress exceeds the closed-form value, which is plausible if the numerical model captures stress concentrations at the constraint and shoulder regions that the plain torsion formula omits. All computed and measured stresses (≤ 10.6 MPa) are far below the allowable value, so the shaft is not strength-critical at 1470 N·mm.

E. Limitations

The following points qualify the case study and should be considered when interpreting it:

1) Scale: A 10 mm shaft at 1.47 N·m is a sub-system example. Its results do not describe the torsional stiffness of the chassis frame, which is governed by the side-rail and cross-member sections and their joints.
2) Deformation definition: The analytical twist implies a surface displacement of about 0.0068 mm at the shaft radius, whereas 0.00499 mm is reported. The point and direction at which deformation is compared should be defined explicitly.
3) Test range: The test extended to 150° twist, well beyond the elastic regime of a 10 mm steel shaft. The elastic comparison applies only to the initial part of the curve, and the load should be reported in torque units (N·m or kgf·m) rather than the logged unit.
4) Speed dependence: At constant load torque, stress and deflection do not depend on motor speed; trends reported against rpm should be explained through the motor torque–speed characteristic.
5) Allowable stress: The 57.5 MPa value is an allowable shear stress derived from a handbook ultimate value with a factor of safety, not a yield strength; von Mises stress should be compared against a yield-based allowable.

6. Research Gaps

Most reviewed studies concern cranes, booms and lifts rather than ladder chassis, and coupling explicit contact modelling, plate buckling, fatigue and stability in a single optimization framework remains an open challenge. Eight specific gaps are identified in Table 7.

ID	Gap	Significance
G1	Few direct HCV chassis torsional optimization studies	Ladder frames experience extreme asymmetric twist and need dedicated analysis
G2	Simplified or rigid joint and pad contact modelling	Rigid ties miss local overlap and bracket stress concentrations
G3	Buckling absent from the optimization loop	Thin walls may shift the failure mode from yielding to panel instability
G4	Fatigue assessed but not optimized	Long service lives under cyclic rough-terrain loading
G5	Limited strain-gauge validation	Rig tests are needed to confirm numerical stress predictions
G6	Inconsistent dynamic load factors (1.15–1.5)	Standard-referenced factors are needed for comparability

All rights reserved by www.ijsrd.com

G7	Mass, stiffness and reliability rarely treated jointly	Robust multi-objective design requires simultaneous reliability checks
G8	Chassis structure and vehicle stability treated separately	Mass changes affect both structural margins and rollover stability

Table 7: Research gaps in HCV chassis torsional optimization

V. Proposed FEA-Based Optimization Workflow

A nine-step workflow (Fig. 3) is proposed to address the identified gaps. Torsional stiffness should be expressed as $K_t = T/\theta$ (N·m/deg), obtained from a unit-twist load case, so that candidate designs can be compared by both K_t and K_t/mass. If the checks at step 8 fail, the design variables and limits are revised and the loop returns to step 5.

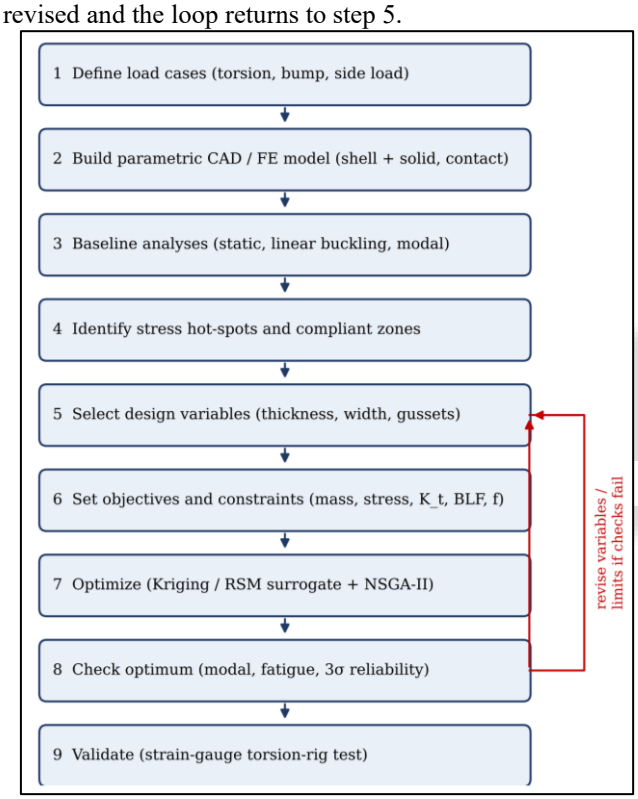


Fig. 3: Proposed FEA-based optimization workflow for HCV chassis torsional stiffness.

The workflow can be organized as the project plan in Table 8, with each stage mapped to the gaps it addresses.

Stage	Activity	Gaps
1	Define chassis geometry and load cases with standard dynamic factors	G1, G6
2	Build parametric shell/solid model with explicit contact and joint elements	G2
3	Run baseline static, linear buckling and modal analyses	G3
4	Screen design variables; build Kriging/RSM surrogates	G7
5	Incorporate buckling load factor and fatigue constraints in the optimization	G3, G4
6	Perform 3σ reliability verification of the optimized chassis	G7
7	Evaluate the effect of mass reduction on rollover stability margins	G8
8	Plan prototype strain-gauge validation	G5

Table 8: Suggested project plan and gaps addressed

VI. Conclusions and Future Work

1) FEA-based optimization of comparable thin-walled structures has achieved mass reductions of about 8–12.5%, typically with thickness and cross-section variables, stress/deflection constraints and, more recently, surrogate-assisted multi-objective search with reliability checks.
2) The shaft and worm-gear case study demonstrates a consistent analytical–FEA–experimental validation chain, with all computed stresses (≤ 10.6 MPa) well below the allowable 57.5 MPa. It addresses a sub-system, however, and does not constitute a chassis-level optimization.
3) Eight research gaps are identified; the most significant for ladder chassis are the lack of direct torsional optimization studies, rigid joint modelling, and the exclusion of buckling and fatigue from the optimization loop.

The proposed nine-step workflow provides a route to close these gaps.

Future work should (i) extend the sub-system model to a full-vehicle multibody framework capturing transient twist; (ii) apply topology and size optimization with evolutionary algorithms to the side rails and cross-members; (iii) evaluate HSLA steels and composites for stiffness-to-weight gains under off-road dynamic loading; and (iv) validate the optimized design by strain-gauge torsion-rig testing on a physical frame.

References

[1] M. Ravi Kumar, K. Rajasekhar and S. Srikiran, "Structural and Torsional Stiffness Analysis of a Heavy Vehicle Ladder Chassis Frame," *Int. J. Mechanical Engineering*, vol. 5, no. 3, pp. 112–118. [details to be verified]
[2] N. V. Hargude and S. N. Sheikh, "Topology Optimization and Material Substitution for Heavy Commercial Vehicle Chassis Frames," *J. Automobile Engineering & Rigor*, vol. 7, pp. 45–52. [details to be verified]
[3] S. P. Kotalwar and S. H. Harje, "Emergency Brake System," *Int. J. Innovations in Mechanical and Automotive Research*, vol. 1, no. 2, 2015.
[4] S. Mahajan and J. Joy, "A Review on Brake Assist System," *Int. J. Engineering Science and Innovative Technology*, vol. 4, no. 3, 2015.
[5] PSG College of Technology, *PSG Design Data Book*, Coimbatore, India, 2011.
[6] Visvesvaraya National Institute of Technology, *Design Data for Machine Elements*, Denett & Company, Nagpur, India, 2011.
[7] R. S. Khurmi and J. K. Gupta, *A Textbook of Machine Design*, S. Chand Publishing, New Delhi.

All rights reserved by *www.ijsrd.com*

[8] K. Singh, *A Textbook of Automobile Engineering*, vol. 1, Standard Publishers Distributors.
[9] Studies cited by author in Sections 3.1–3.3 (Thivagar; Raghunath Reddy and Naidu; Dharia and Bhopale; More; Kotalwar and Harje; Joy et al.; Thakur et al.; Saini and Joshi; Belhocine et al.; Nayak; Wakchaure et al.; Jia and Wan; Fang et al.; Sun et al.; Cao et al.): full citations to be added from the original sources.

All rights reserved by *www.ijsrd.com*